J. Fluid Mech. (1986), *vol.* 173, *pp.* 357–386
Printed in Great Britain

The fractal facets of turbulence

By K. R. SREENIVASAN AND C. MENEVEAU
Center for Applied Mechanics, Yale University, New Haven, CT 06520, USA

(Received 25 March 1986)

Speculations abound that several facets of fully developed turbulent flows are fractals. Although the earlier leading work of Mandelbrot (1974, 1975) suggests that these speculations, initiated largely by himself, are plausible, no effort has yet been made to put them on firmer ground by resorting to actual measurements in turbulent shear flows. This work is an attempt at filling this gap. In particular, we examine the following questions: (*a*) Is the turbulent/non-turbulent interface a self-similar fractal, and (if so) what is its fractal dimension? Does this quantity differ from one class of flows to another? (*b*) Are constant-property surfaces (such as the iso-velocity and iso-concentration surfaces) in fully developed flows fractals? What are their fractal dimensions? (*c*) Do dissipative structures in fully developed turbulence form a fractal set? What is the fractal dimension of this set? Answers to these questions (and others to be less fully discussed here) are interesting because they bring the theory of fractals closer to application to turbulence and shed new light on some classical problems in turbulence – for example, the growth of material lines in a turbulent environment. The other feature of this work is that it tries to quantify the seemingly complicated geometric aspects of turbulent flows, a feature that has not received its proper share of attention. The overwhelming conclusion of this work is that several aspects of turbulence can be described roughly by fractals, and that their fractal dimensions can be measured. However, it is not clear how (or whether), given the dimensions for several of its facets, one can solve (up to a useful accuracy) the inverse problem of reconstructing the original set (that is, the turbulent flow itself).

1. Introduction

Starting with Richardson (1922), it has been thought that fully developed turbulence consists of a hierarchy of eddies, or scales of various orders. The mechanism responsible for this situation is assumed to be that eddies of a given order (or size) arise as a result of the loss of stability of larger eddies of the preceding order; these in turn are assumed to lose their stability and generate eddies of a smaller order to which they transmit their energy. This recurring scheme is expected to terminate at scales small enough to be stable – that is, scales whose characteristic Reynolds number is unity. It is well known that this lower bound on the scale size is of the order of the Kolmogorov scale. This theory of cascade, verbalized in a memorable rhyme by Richardson (1922), and cultivated by Kolmogorov (1941, 1962), Obukhov (1941, 1962), Onsager (1945) and Weizsäcker (1948), has made remarkable strides in advancing our understanding of turbulent flows.

It is this description of turbulent flows – namely that they are 'objects' consisting of a hierarchy of scales – that leads to the expectation that the theory of fractals (Mandelbrot 1982, to which reference must be made for an enjoyable and original account of fractals) must be applicable to turbulence. In the most basic sense, fractals

are objects that display self-similarity over a wide range of scales. (We shall return in §5 to the fact that fractals are now used to describe more general class of objects than those displaying strict self-similarity.) Mandelbrot (1982), for example, has remarked that 'turbulence involves many fractal facets' and claimed that a proper investigation of the geometric aspects of turbulence – which has been ignored all along in the vast literature on turbulence – must necessarily involve fractals; concepts from Euclidean geometry are totally inadequate. He has also led the way by his own investigations (Mandelbrot 1974, 1975) but, in his own words (Mandelbrot 1982), 'they involve suggestions with few hard results as yet.' The intention of this paper is to remedy this situation by resorting to actual measurements in turbulent flows.

Analogous to the Euclidean dimension of classical (or ordinary) objects, each fractal object is associated with a characteristic dimension called the fractal dimension which forms a basic measure of it fragmentation or roughness; it has the property that it is strictly greater than the object's topological dimension. It appears as a certain exponent $D = \log N/\log(1/\epsilon)$, characteristic of a self-similar object which is made of N parts, each of which is obtained from the whole by a reduction of ratio ϵ. (We hope that this inadequate explanation here, to be amplified in later sections, will not hinder the readability of this paper.) Of course, a complete description of fractal sets demands a specification of other quantities such as lacunarity (Mandelbrot 1982) – which, loosely speaking, is a measure of how far the fractal object is from being dust-like – or the entire spectrum of scaling functions (Halsey *et al.* 1986) only one of which is the fractal dimension. (Even more appropriately, one may use scaling functions of the type introduced by Feigenbaum 1983; these scaling functions contain all the geometric information about the object in question, but they are nowhere differentiable and are awkward to handle – even assuming that they can be constructed somehow.) Our primary effort in this paper will be confined to the determination of the fractal dimensions (if they exist) of the turbulent/non-turbulent interface (§2), iso-velocity surfaces (§3), and regions of active dissipation (§4); in §5, we briefly discuss several other avenues, studied to date in less detail than the issues of the preceeding three sections. In each section, we lay sufficient foundation for the specific issues to be discussed there. Section 6 will put these various measurements in the overall context of what additional insight one may acquire about turbulent flows.

2. Fractal dimension of the turbulent non-turbulent interface

2.1. *Background*

Observations (Corrsin & Kistler 1954) suggest that in high-Reynolds-number unbounded turbulent shear flows a sharp front or interface demarcates the turbulent and non-turbulent regions (see figure 1). The free edge of a boundary layer shows much the same behaviour. Townsend (1956) suggested that large eddies of turbulence contort the interface, but a visual or spectral study of the interface suggests that contortions over a range of scales occur. In the framework of scale similarity alluded to above, this leads to the natural expectation that the interface is a fractal surface. The aim in this section is to determine the fractal dimension (if one exists) of the turbulent/non-turbulent interface in several classical shear flows.

It is generally understood that turbulent/non-turbulent interface means the surface separating the vortical and non-vortical regions of the flow; the vortex-stretching mechanism inherent in three-dimensional motion can be thought of as

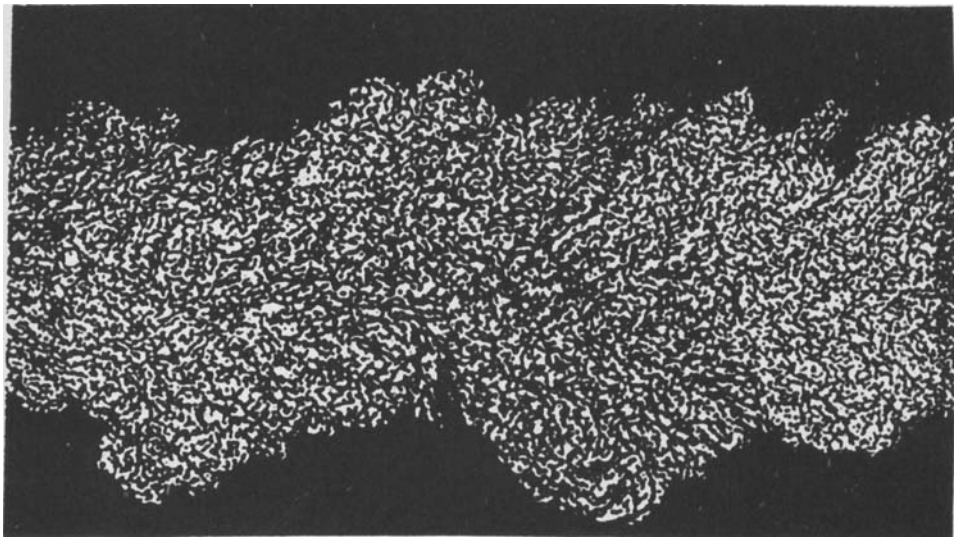

FIGURE 1. A short duration shadowgraph of the wake of a projectile shot through the atmosphere at supersonic speed. This classic photograph made at the Ballistic Research Laboratories, Aberdeen Proving Ground, first appeared in Corrsin & Kistler (1954), and has since been reproduced many times. The remarkably sharp boundary between the turbulent region in the wake and the outside air has led to the notion of a contiguous interface whose properties were explored by Corrsin & Kistler, and several others later.

being responsible for maintaining a sharp separation between the two regions. That such a surface can be defined was demonstrated by Corrsin & Kistler (1954), who also studied its properties in some detail. It is by no means obvious that the interface observed in flow-visualization pictures such as figure 1 and the vortical/non-vortical interface are the same. We shall return to this point later but, until required, we shall not be specific about which interface we are discussing.

The prescription for determining the fractal dimension of the interface (surface) is to cover it with area elements of decreasing size, and note how the area changes with the resolution ϵ of these square elements. For a surface that is highly contorted with squiggles of ever-increasing fineness, the measured area estimates will increase indefinitely with increasing resolution. If the surface has no regularity associated with it, one cannot in general specify the manner in which the area will increase with increased resolution. However, if some order prevails in the sense that the surface observes scale similarity – that is, the surface looks the same (at least *statistically*) at all levels of resolution, or, equivalently, it is a self-similar fractal – the area increase will follow a power law; in general, power laws are symptomatic of self-similar or fractal behaviour. For a true fractal surface of dimension D_3 (the suffix 3 indicating that the interface is embedded in a three-dimensional physical space) the area will indefinitely increase according to the relation

$$N = \epsilon^{-D_3}. \tag{2.1}$$

One can rewrite (2.1) as

$$D_3 = \frac{\log N}{\log (1/\epsilon)}. \tag{2.2}$$

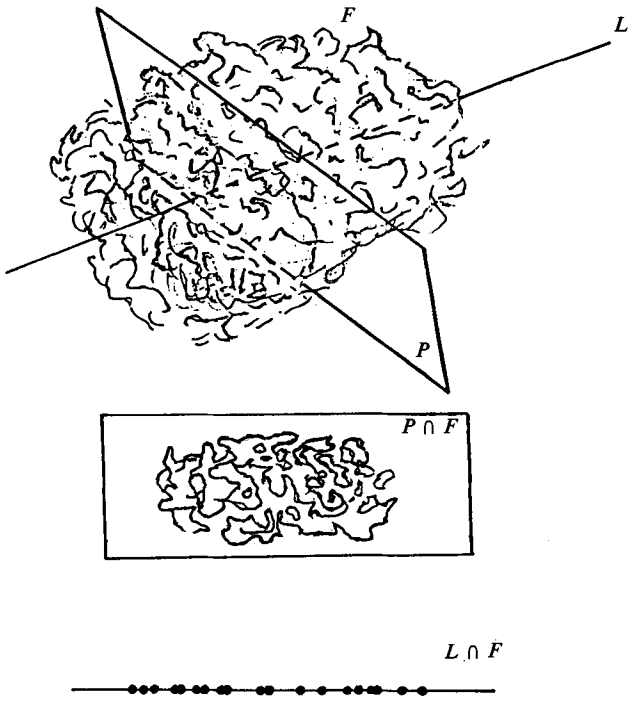

FIGURE 2. A schematic of an object F with a fractal interface, and its intersections with a plane and a line. The intersection with the plane leads to an object whose border has a dimension D_2, one less than D_3, the dimension of F embedded in the three-dimensional space. The dimension of the line intersection leads to a Cantor set whose fractal dimension D_1 is 2 less than D_3.

This is the standard relation used in fractal-dimension calculations. The meaning of the dimension becomes clearer if we apply this above procedure to classical surfaces, say a square of unit area. Let us cover the square with 16 area elements each of which is of length $\frac{1}{4}$. Then D_3 will be $\log 16/\log \frac{1}{4} = 2$, which is the dimension of the area of surface in Euclidian geometry. It is trivial to convince oneself that covering the square with increasingly finer area elements will always give $D_3 = 2$ for the square. From this simple example and other similar ones, one concludes that for classical surfaces the dimension calculated from (2.2) has the usual meaning associated with the dimension. For fractals, the dimension as calculated from (2.2) will in general not be an integer – and hence the name fractal – but it retains the meaning as the exponent specifying the rate at which the number N of area elements increases with ϵ. As already noted, a characteristic of a fractal surface is that its fractal dimension will be larger than its Euclidian dimension of 2. What this implies is that a fractal surface covers something between an area and a volume, a fact for which the large degree of convolutedness of the surface is responsible.

What use is the fractal dimension of a fractal surface since its surface area is undefined? From (2.1) it is seen that, given the accuracy (or the resolution) to which the area needs to be specified, the dimension D_3 will provide the number of the area elements of prescribed resolution required to cover the fractal surface. This goes some way in describing the fractal surface. A complete specification of the fractal surface no doubt requires additional information, such as the location and the orientation of these little area elements, but the dimension is the basic quantity related to the

convolutedness of the surface. A measure of the convolutedness of a surface is of importance, for example, in the contexts of combustion.

2.2. *Dimension from sections with lower-dimensional subspaces*

To measure the fractal dimension of a surface by the direct procedure described above is difficult, and so we adopt alternative procedures based on sections with lower-dimensional subspaces (Mandelbrot 1982). To explain this, it is convenient to refer to figure 2. Let F be an object (e.g. a turbulent jet) in three-dimensional space with a fractal interface of dimension D_3. Let P be a plane intersecting the object. In analogy with our experience in Euclidean geometry, we may expect that the fractal dimension D_2 of the boundary of the resulting object $P \cap F$ and the dimension D_3 are related by

$$D_3 = D_2 + 1. \tag{2.3}$$

Similarly, an intersection of the object F with a line element gives a set of isolated points – akin to the Cantor discontinuum – whose dimension D_1 can be measured. Again, in analogy with classical objects, we expect that

$$D_3 = D_1 + 2. \tag{2.4}$$

Although there are exceptions to this rule (Mandelbrot 1982, p. 135), it is known to hold if the sections taken are independent of the fractal itself. Equivalently, the orientation of the intersecting plane or line will be irrelevant if the fractal is isotropic. More discussion and a brief circumstantial justification of this point will appear in §§2.3 and 2.4.

It is appropriate to mention here that the interface cannot be a true fractal because the scale similarity at all scales, leading to one fixed value of D_3, does not strictly obtain. Clearly, it will be truncated on the low end by the Kolmogorov scale; that is, if one measures the area of the interface with resolutions better than the Kolmogorov scale, it behaves like a classical surface of finite area (because surface convolutions on even finer scales do not exist). On the upper end, it can be expected to be bounded by scales comparable with or smaller than the large scale of the flow. Thus, the interface can be expected to be fractal-like only in an intermediate range of scales†. This is not a highly restrictive situation because, in all practical circumstances, there are inevitable scale cutoffs, and any meaningful application of the fractal concept to real circumstances will have to live with this fact. At large flow Reynolds numbers, the range of scales over which similarity can be expected to hold is large; and, naturally, it is easier to identify the fractal-like behaviour. As will be described more fully at appropriate places, instrumentation constraints restricted our experiments to moderate Reynolds numbers (the integral to Kolmogorov scale ratio no more than a few hundreds). Even so, the results are sufficiently convincing to justify their publication: besides making the important connection between fractals and fluid flows, they shed new light on some classical problems of turbulence.

2.3. *Dimension by intersection with a plane*

The practical way of obtaining two-dimensional sections or slices would be to seed the flow with some passive markers (e.g. smoke), illuminate a section of the flow by a thin sheet of light, and photograph the section for later analysis, namely measuring

† It is worth pointing out that, while the large scale is set by the flow boundary conditions and the small scale by the viscosity of the fluid, the equations of motion themselves do not set any new scales, which is what renders the scaling expectations plausible.

FIGURE 3. A smoke photograph of a turbulent boundary layer developing on a flat plate. The momentum thickness Reynolds number is around 2000. The thickness of the intersecting light sheet is of the order of the Kolmogorov thickness.

the dimension of the 'border' between the turbulent and non-turbulent regions. Although the intersecting plane must in principle be mathematically thin, it may in practice be of finite thickness without violating this principle, provided the thickness is smaller than or comparable with the Kolmogorov lengthscale η. The rationale for this assertion is that the 'fuzzing' due to the finite thickness of the plane is negligible because the Kolmogorov thickness represents the smallest scale of motion relevant to turbulence dynamics.

We have already alluded to the fact that smoke pictures (or pictures obtained by any other means of flow visualization) do not mark vorticity regions (which they should, to be truthful to the interface) for the following two reasons, both related to the diffusivity of the passive marker. If we remember that smoke is composed of aerosols (= oil fog) whose diffusivity is small compared with the molecular viscosity, the relatively large value of the effective Schmidt number will create a disparity between the smallest dynamical scale (i.e. η) and the smallest scale visible in the flow. This is not too worrisome as long as the latter is smaller than the former. The second, and more important, point is that to mark the interface satisfactorily, one has to put smoke exactly where vorticity is being generated, which is strictly impossible. Obviously, if one puts smoke very far upstream of the observation point, the pattern one sees is in general a remnant of the integrated memory that a given streakline experiences, and not necessarily a reflection of the local dynamics and geometry. Because turbulence diffuses smoke rather rapidly, there is some hope, however, that it will *roughly* mark the interface if carefully injected in the fully turbulent region reasonably close to the region of visualization, but not so close that it does not have time to diffuse.

Even if one grants the plausibility of this last statement, even roughly marking the interface by smoke is admittedly a trial-and-error procedure in practice. The issue is worth exploring in detail – which we have not done – but there are reasons of precedence which are somewhat reassuring. For example, the statistics of the interface obtained by marking it with hydrogen bubbles (Kim, Kline & Reynolds 1971) and by heat (Sunyach & Mathieu 1969) agree favourably with those obtained by momentum and other means; we ourselves have recorded elsewhere (Sreenivasan, Antonia & Britz 1979) some simultaneously obtained traces of two components of fluctuating velocity, Reynolds shear stress and the temperature fluctuation in a

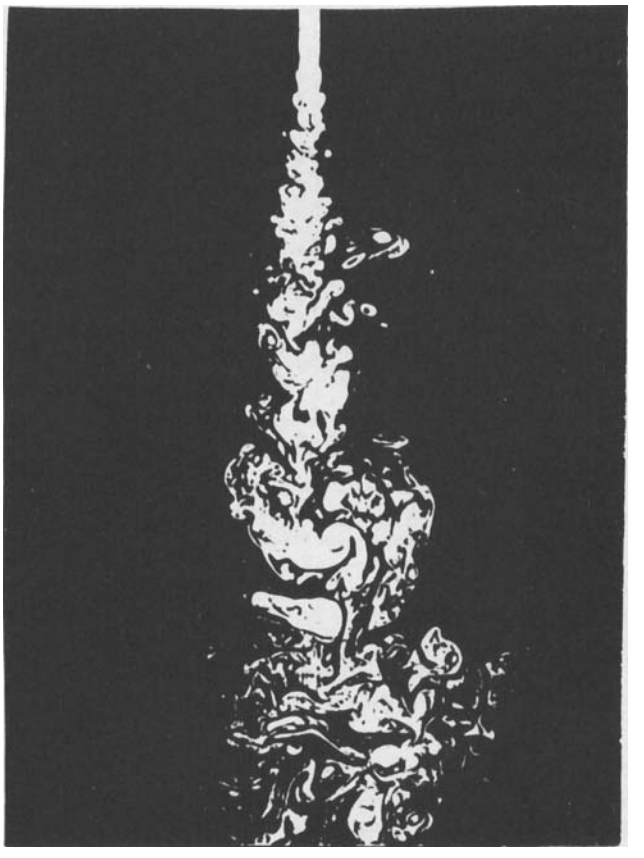

FIGURE 4. A section of an axisymmetric jet made visible by laser-induced fluorescence, from Dimotakis *et al.* (1981). Scales down to the Kolmogorov limit have been resolved in this picture.

slightly heated jet, which confirm that passive scalars are useful for marking the interface. The final point must no doubt be that, although our procedure is believed to mark the interface roughly, it is the smoke/no-smoke interface that we are strictly studying.

Another concern is that a streamwise section is somehow preferential, thus biasing the results. To test this, one ought to take plane sections of the interface at several orientations and demonstrate the invariance of the results. For the anisotropic flows of the sort studied here, it is possible that the scale-invariance concept must be thought through more thoroughly, and that one may come up with more than one fractal dimension depending on which planar section one is measuring. Our work in this direction is continuing, but our argument is that the present results are representative.

Figure 3 shows a section of a boundary layer made visible by injecting smoke. This figure appears to suggest that there is no contiguous interface, and that there are islands of non-turbulent regions surrounded by turbulent ones, just as there are isolated pockets of turbulence sticking out. The reason that photographs like figure 1 do not show this feature is that they have been obtained by optical means which integrate along the path of light. Obviously, this will smooth out the interior 'holes', and what one sees as a contiguous interface is the horizon of a large number of images

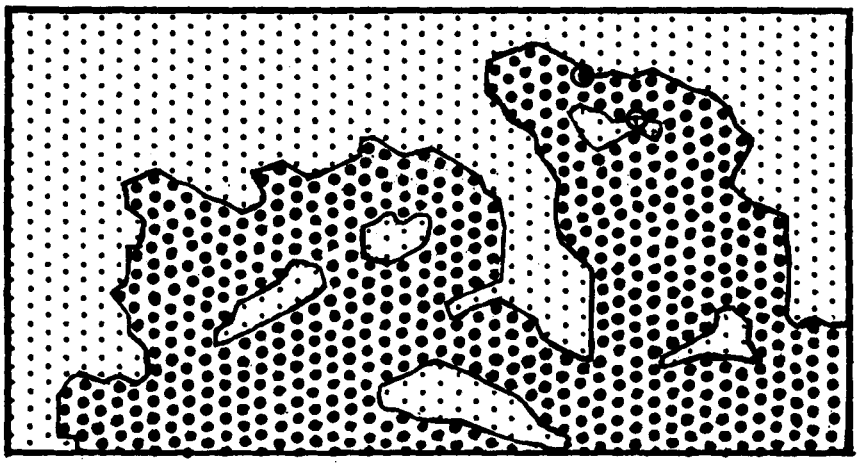

FIGURE 5. A schematic of a part of a digitized image. The dark dots represent the points with intensity above threshold (turbulent regions, by definition here), the light ones representing non-turbulent regions. We want to measure the fractal dimension of the border between the two regions. The little circles of radius ϵ drawn around a dark and a light dot in the upper right corner are two examples of boundary points within the distance ϵ.

superposed on each other. Dimotakis, Lye & Papantoniou (1981) pointed out this fact first, and produced several fascinating pictures of a turbulent jet, one of which is reproduced here as figure 4. (No analysis was attempted by us on the pictures obtained by these authors.) Plane sections by themselves cannot deny the existence of out-of-plane connections of what appear as islands or holes, and we should emphasize that to prove the non-contiguity of the interface one has to produce at the very least simultaneous pairs of pictures in perpendicular planes. In the absence of such work, the point is made here for the sole purpose of indicating that, if the interface is indeed non-contiguous, the fractal dimension one obtains will not lose its meaning but will have to be interpreted as a measure of both its 'roughness' and 'fragmentation', and not merely of the former, as would be the case for a contiguous interface.

We may now discuss several ways in which the fractal dimension D_2 of the border can be measured. The length of the border, in analogy with the coastline of an island cluster, increases with increasing resolution according to the relation

$$L = K\epsilon^{1-D_2}, \tag{2.5}$$

where ϵ is the lengthscale relating to the fineness of resolution, and K is a constant related to the lacunarity of the fractal set. This direct method has so far eluded us chiefly because of the algorithmic complexity in faithfully following the highly contorted, multivalued and disconnected interface (see figures 3 and 4), and alternatives seem called for. We have adopted a simple alternative spelt out in Mandelbrot (1982) and Grebogi *et al.* (1985), but summarized here with the anticipation that they may be unfamiliar to a number of the Journal's readers.

Considering both regions (turbulent and non-turbulent) that are within a distance ϵ from the border, one can form a strip of width 2ϵ about the border, which will have an area of $2\epsilon L$, where L is the length of the border. This area clearly goes like ϵ^{2-D_2}, from (2.5). One measures this area for varying ϵ, and obtains D_2 from the slope of a log–log plot. The implementation of this idea involves the following procedure. One

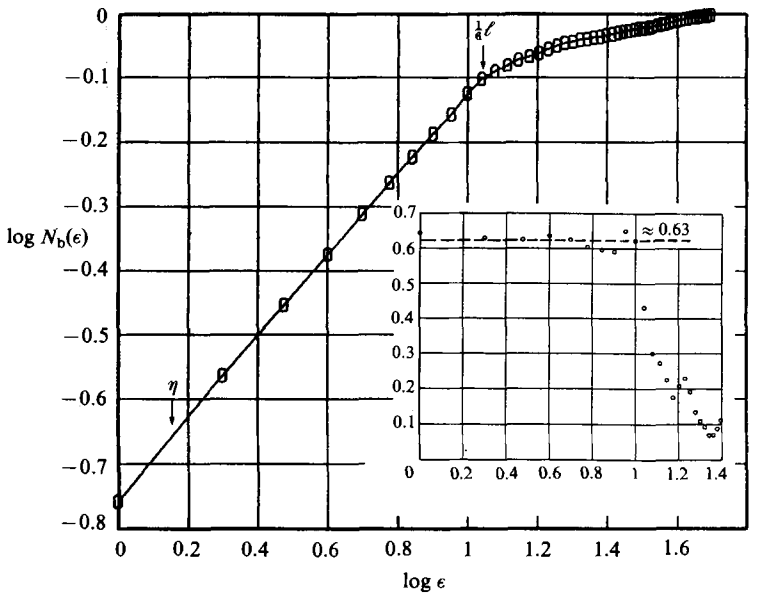

FIGURE 6. The logarithm (to base 10) of the number of boundary points N_b (see figure 5) as a function of the distance ϵ from the boundary. The flow is a heavily tripped boundary layer, thickness about 10 cm, $U_\infty = 2.5$ m s^{-1}. The Kolmogorov and the integral scales are shown for reference. The inset showing the slope gives $D_2 = 2 -$ mean slope $= 1.37$; D_3 is thus expected to be 2.37.

digitizes the image of the flow obtained as described previously, and obtains an assignment of light intensity at each of the digitized points. One then sets a judicious threshold for the light intensity which demarcates the turbulent (above-threshold) from the non-turbulent (below-threshold) regions. (Naturally, one has to ascertain that the precise value of the threshold is not important for the results to follow, and evidence to this end will be presented at the appropriate place.) One then obtains a digitized image, schematically shown in figure 5, where each dark dot is a digitized image point in the turbulent region and each light dot in the non-turbulent. It is the dimension of the border between the two regions that we want to measure. The conceptual equivalent of the data processing on the computer is the following. Draw around each of these digitized points (dark as well as light) circles of radius ϵ. Whenever a circle drawn around a point crosses the border, obtained by interpolation between the neighbouring light and dark dots, the point is counted as a border point within a distance ϵ from the border. Count the number of all border points $N_b(\epsilon)$ within the distance ϵ from the border. Repeat the process for varying ϵ, and determine the variation of $N_b(\epsilon)$ with respect to ϵ. From the earlier discussion in the paragraph, we have

$$N_b(\epsilon) \propto \epsilon^{2-D_2}. \tag{2.6}$$

For future reference, we may note that the quantity $2-D_2$ (or in general $d-D_d$, where D_d is the fractal dimension of the object's interface in the embedding space of dimension d) is called the codimension. In most well-behaved (i.e. integrable or non-chaotic) systems, a small amount of uncertainty ϵ in the initial state will translate to a comparable final-state uncertainty. For fractal objects, the final-state uncertainty is large and proportional to ϵ^{D_c}, where D_c is the codimension (Grebogi *et al.* 1985). The codimension appears again in §4.

Figure 6 shows a plot of log $N_b(\epsilon)$ *vs.* log ϵ obtained from the digitized image of the

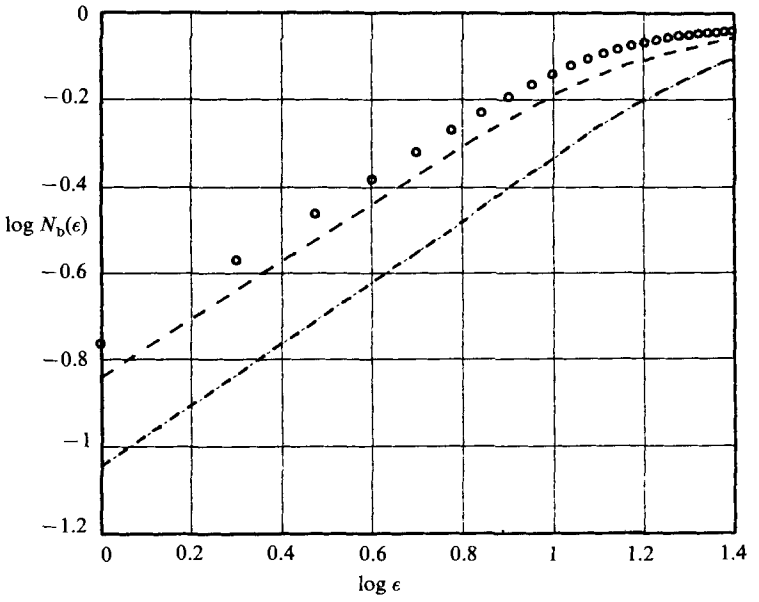

FIGURE 7. The effect of threshold setting on the codimension. The threshold (in the notation of the text) varies by a factor of 1.5 with no perceptible change in the slope. In the units described in the text, the thresholds are (from top to bottom) 3000, 3500 and 4000.

type shown in figure 3; the inset shows the slope of the curve. Clearly, there is a region of constant slope as expected for a fractal interface. Several comments must be made before interpreting the result. First, the low end of the constant-slope region is comparable with the Kolmogorov scale†. The high cutoff seems to occur around $\frac{1}{6}\ell$, where ℓ is the transverse integral scale of turbulence in the boundary layer. (This integral scale was obtained from two-point correlation measurements with the fixed probe at $y/\delta = 0.4$ and the other probe moving outwards.) The obvious conclusion that the scale similarity extends only up to $\frac{1}{6}\ell$ on the high end is not correct because, as we shall soon show, the high cutoff occurs prematurely because of the limitations of the image processing procedure. To obtain reliable statistics on the high end, one has to include many large scales in the digitized image, which is usually hard (especially if the fine resolution requirements are to be satisfied also) because of the finite capacity of the image digitizer. We have not been able to do that, which means that the apparent termination of scale similarity at $\frac{1}{6}\ell$ is artificial. This shortcoming is overcome in the line-intersection method of §2.4.

The second comment relates to the effect of the threshold setting on the slope in figure 6. At least within the threshold range of 3000–4000 for the light intensity (the units being such that 12000 indicates the brightest spot in the picture and 0 the darkest), the power of ϵ in (2.7) is essentially constant (figure 7); the threshold of figure 7 is about $\pm 15\%$ of that used in the boundary-layer work. The third relevant

† There is some concern that to detect similarity on scales of the order of η, the resolution of the digitized image must be substantially smaller (at least by a factor 2). Figure 6 shows that this factor is about 1.5 for present measurements. We may remark that estimating η to an accuracy better than a factor 2 is beset with many uncertainties; among other things, it depends on the precise location in the flow, the assumptions made in obtaining the energy dissipation, the probe size, etc. The number quoted in figure 6 is thus a representative value.

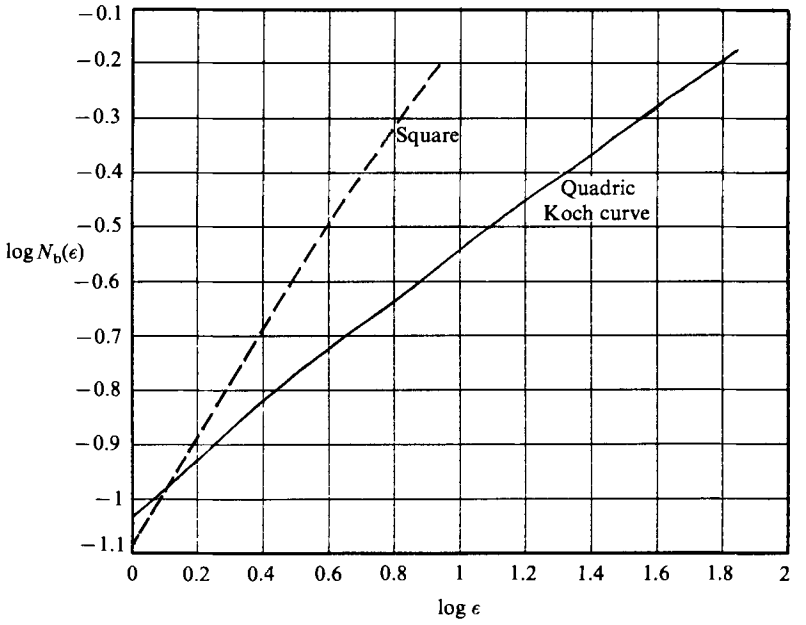

FIGURE 8. Calibration experiments for the imaging method. The continuous line (mean slope = codimension = 0.5) is for a quadric Koch island, and the dashed line (codimension = 1) is for a square. Their respective dimensions are in good agreement with the theory.

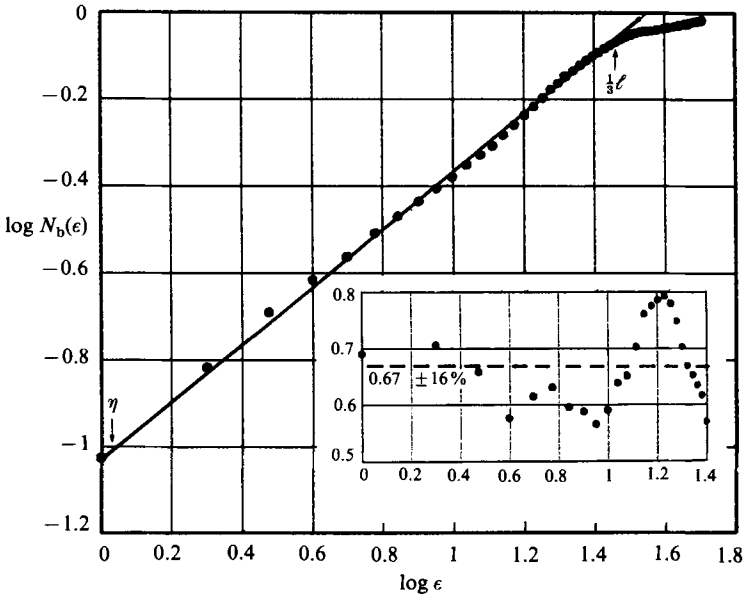

FIGURE 9. The logarithm (to base 10) of the number of boundary points N_b (see figure 5) as a function of the distance ϵ from the boundary. The flow is a round water jet seeded with polystyrene spheres. Jet exit Reynolds number is about 2500, diameter $D = 5$ mm; $x/D = 30$. The inset shows that the slope of the line is $0.67 \pm 15\%$.

comment concerns the 'calibration' experiments on some well-known fractals (e.g. a quadric Koch island, Mandelbrot 1982, p. 50) and regular objects (such as a black square). As shown in figure 8, it is clear that the codimension (mean slope of the curves) is 0.5 for the Koch island (i.e. $D_2 = 1.5$, the theoretical value), and 1 for the square ($D_2 = 1$).

Putting all this together, we conclude from figure 6 that scale similarity extends from η up to a fraction of ℓ (the precise value to be determined shortly), and that we have $D_2 = 2$-slope $= 1.38$ (for the border), leading to the conclusion that $D_3 = 2.38$ (for the interface surface).

Figure 9 shows similar data for an axisymmetric jet of water flowing vertically down into a large tank of still water. The jet was seeded with polystyrene microspheres; both seeding and gravity effects were considered negligible. A part of the jet in the developed region (in the vicinity of $x/D = 30$) was intersected by a thin sheet of light, photographed and digitized as before. Again, scale similarity extends all the way from η to a fraction of ℓ; for reasons already mentioned, we think little of the fact that the high cutoff occurs at $\frac{1}{3}\ell$ (instead of $\frac{1}{6}\ell$ in the boundary layer) or that the slope is slightly different from the boundary-layer case. This latter is well within the scatter of the data (about which more will be said in §2.4).

In determining the dimension, we have chosen to digitize certain regions of the cross-section that are neither too close to wall (or jet axis) nor too far away from it. Both for the jet and the boundary layer, the digitized image spans (approximately) $0.6 < \gamma < 0.1$, where γ is the intermittency factor representing the fraction of time the flow is turbulent at a given point in the flow. We empirically found the region just mentioned to be optimum given the image-processor constraints.

2.4. *Dimension by line intersection*

As discussed earlier, the dimension of the set resulting from line intersection of the interface (yielding simply a 'truncated' Cantor set of dimension less than 1) is expected to be two less than that of the interface, D_3. In practice, we have interpreted that this statement holds true for the one-dimensional cut obtained by intersecting a *moving* interface with a small (i.e. η or smaller) stationary hot-wire probe. This assumes the validity of Taylor's frozen-flow hypothesis, which we know is not strictly true, but much can be learnt in spite of this shortcoming.

As is standard in the turbulence literature, we formed the intermittency function from the measured velocity signal by setting a convenient threshold and a hold time. The reasonableness of the threshold as well as the hold time was ascertained by a comparison of the resulting intermittency function with the original signal. The set of intersection points between a horizontal line and the intermittency function results in a 'truncated' Cantor set whose dimension D_1 we want to measure. To obtain D_1, the so-called box-counting algorithm, which is merely the application of (2.2) for line elements, has been employed. It makes direct use of the definition of fractal dimension by counting the number N_ϵ of the line segments of length ϵ required to cover the set for several values of ϵ.

Figure 10 shows a typical set of data for N_ϵ *vs.* ϵ for the boundary-layer flow. It is seen that there is a sizeable region of constant slope, giving in this instance $D_1 = 0.4$; we infer that $D_2 = 1.4$ and $D_3 = 2.4$. It should be noted that D_1 inferred from one-dimensional cuts is approximately one less than D_2 inferred from intersections with planes, thus providing some circumstantial justification for the method of sections with lower-dimensional subspaces discussed in §2.2. Note also that the region of self-similarity does not extend all the way down to η as in the two-

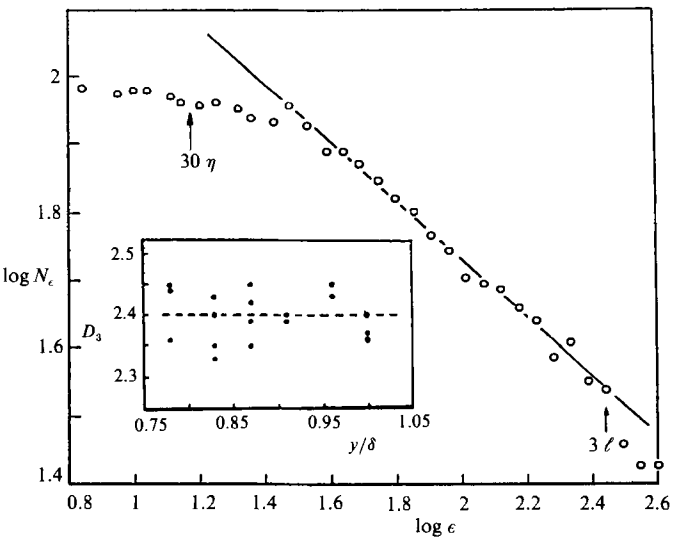

FIGURE 10. The logarithm (to base 10) of the number of segments N_ϵ of length ϵ needed to cover the Cantor discontinuum formed by the intersection between a horizontal line and the intermittency function (turbulent boundary layer, $y/\delta = 0.91$, $U_\infty = 12$ m s^{-1}). The inset shows the dimension D_3 as a function of the position of the line intersection, or probe height from the wall in the boundary layer, obtained for several chunks of data. Corresponding intermittency factors, from the highest to the lowest, are: 0.41, 0.24, 0.19, 0.13, 0.10, 0.08.

dimensional slice method of §2.1, and even scales up to 30η do not fall on the straight part. Part of the reason is clearly the problem related to Taylor's hypothesis and the size of the hot-wire, which is several η long (approximately 10η in this case) both of which will bias the results at small scales. A more basic problem is related to the inappropriateness of using the streamwise velocity for constructing the intermittency function. One should ideally use a vorticity probe (which gives a much clearer on–off signal), or a passive scalar that is uninfluenced by the long-range effects of the turbulent pressure field. However, the outer cutoff does not occur until ℓ or beyond. Combining this result with the inner cut-off of the previous subsection, we might conclude that scale similarity extends between η and 3ℓ. (The outer cutoff is thus approximately the streamwise integral scale, which is of the order of the boundary-layer thickness.)

It is now helpful to examine the sensitivity of the dimension results with respect to position in the intermittent region where the one-dimensional slice was obtained. The inset in figure 10 shows the data as a function of the probe height in the intermittent region of the boundary layer. Because the interface is rarely found deep in the flow, not surprisingly, we cannot compute the dimensions for $y < 0.5\,\delta$ (corresponding to a γ of almost unity). In fact, calculations become uncertain for $y < 0.7\,\delta$ (or, roughly, $\gamma > 0.6$), say, and hence we have not presented any results there. The variability of D_1 is about 10% in the region $0.75 < y/\delta < 1.0$ where the measurements are trustworthy; further, it is approximately in this region that the two-dimensional slices were taken. Clearly, then, this latter method may be expected to represent an average of values obtained from one-dimensional slicing; it is somewhat reassuring that this is indeed the case. We conclude that one-dimensional cuts offer a reasonably valuable tool. The main contribution of this method has been

Flow	Fractal dimension of interface (surface) by two-dimensional slicing	Fractal dimension of interface (surface) by one-dimensional slicing
Boundary layer	2.38	2.40†
Axisymmetric jet	2.33	2.32†
Plane wake	—	2.37‡
Mixing layer	—	2.40‡

† Typical average over a range of the outer flow.
‡ Single value at some typical location in the outer region.

TABLE 1. Summary of the fractal dimensions of the turbulent/non-turbulent interface in several classical turbulent flows

to show that scale similarity extends all the way up to about the integral scales of motion. Recalling that the larger eddies, which are highly dependent on the boundary conditions for the flow, are a few integral scales long, we infer that the scale similarity does not include the biggest scales in the flow. Our conclusions about the interface are summarized in table 1.

From here, the interface dimension of about 2.3–2.4 is seen to be essentially independent of the type of flow. What this means is that one cannot conveniently assign a distinct fractal dimension to each of the different classes of flows. We reiterate that this is not surprising because scale similarity does not encompass the largest scales, which are the ones that depend strongly on the geometric aspects of the flow.

To the extent that in both methods we have examined the interface approximately in the region $0.6 < \gamma < 0.1$, we are not completely justified in talking about the dimension of the interface as a whole, although we expect that what is true of the part is true of the whole. We have already commented on the constraints in the plane-intersection method. One runs into two problems in the line-intersection method. Outside the region we have covered, the infrequent appearance of the interface there would demand the inclusion of data for long intervals of time in order to obtain reliable statistics, and this violates Taylor's frozen-flow hypothesis. This is relatively easy to overcome, at least in principle, by resorting (for example) to intersection by a suitable laser beam of a fluorescing flow. Although this should be attempted soon, we have not done it immediately because waiting for enormously long times results in a randomization of results that will obscure the fractal nature; this point is best deferred to §3 where it is more fully discussed.

Finally, it may be worth remarking that Maxworthy (1986) finds $D_2 = 1.37$ for the interface of the flattened bubbles of air injected into a viscous fluid contained in a Hele-Shaw experiment.

2.5. *Fractal dimension of clouds: a brief comparative study*

Lovejoy (1982) obtained the fractal dimension of clouds using the so-called area-perimeter rule (Mandelbrot 1982, p. 112). For classical objects, the perimeter P and the area A are related through $P \propto A^{\frac{1}{2}}$. For an object with a fractal boundary of dimension D_{2p}, the relation is modified to $P \propto A^{(\frac{1}{2})D_{2p}}$. Thus, if one has different sizes of statistically similar fractal objects, this area-perimeter rule (both P and A evaluated to the same resolution) can be used to determine D_{2p}. Lovejoy used digitized images of satellite and rain-pattern pictures of clouds with sizes varying

between 1 km and 1000 km, and obtained the fractal dimension of about 1.34. It is the coincidence of this number with that obtained by us for D_2 in laboratory turbulent flows that calls for specific comment. Recall that we took a slice of the flow to obtain D_2, whereas Lovejoy was looking at the boundary of the projection of a cloud onto a horizontal plane. The key question then is the difference between the two techniques. We know of no rigorous analysis of this point. However, a projection can be thought of as superposition of a large number of sections, each section being separated from the other by distances of the order η.

Going back to figures 3 and 4, we may qualitatively perceive the effect of superposition of several sections. One effect is obviously to reduce the interior fragmentation (leading to a reduced fractal dimension), but the other effect is to increase the boundary roughness (leading to an increase in fractal dimension). It is the net effect in which we are interested. If the fractal dimension is small (that is, neither the interior fragmentation nor the boundary convolutedness is very large), D_2 and D_{2p} cannot be very different. While taking sections of clouds is not within our capability, superimposing sections of boundary-layer or jet flows can easily be done by increasing the thickness of the light sheet. This has been done, and the result is that increasing the relative size of the light-sheet thickness (from between 1 and 2η to about 5η) increases the dimension D_2 (from 1.37 to 1.43), suggesting that $D_{2p} > D_2$. In doing this experiment we could not unfortunately hold the Reynolds number constant, but if we believe that the primary effect of increasing the Reynolds number is to increase the range of scale similarity (but not alter the dimension), this increase in D_2 is conclusive enough. If this reasoning holds for clouds, we may conclude that $D_2 < 1.34$. It is interesting that Carter *et al.* (1986), using an entirely different procedure from Lovejoy's, arrive at a number of 1.16 for D_2.

We have become aware from a preprint by Lovejoy & Schertzer (1986) that smaller dimensions than 1.34 have in fact been obtained for clouds by setting the threshold to higher values. The result that the more intense regions of a fractal are distributed on sets with lower fractal dimensions is described in §§ 3 and 4.3, and is apparently quite general (Halsey *et al.* 1986).

3. Dimension of iso-velocity surfaces in boundary layers

Here, we seek the fractal dimension of surfaces separating regions of velocity above and below a certain chosen level, say u_1 in figure 11. One can similarly (and more satisfactorily) address the issue of iso-concentration surfaces. We have used the line-intersection method described in §2.4. As before, we get Cantor discontinua whose dimension can be obtained by the box-counting method. The hope is that adding 2 to the numbers obtained will yield the fractal dimension of iso-velocity surfaces; again, one should keep in mind the various aspects discussed in §2. Figure 12 shows results from a box-counting algorithm implemented on a signal obtained in a boundary layer at a height of 0.35δ. The different curves are for different segments of the same (long) signal. To within the variability of about 12%, the line drawn through these various curves represents a mean behaviour. Such results can be obtained for several velocity levels of the same signal (the uncertainty is largest for levels near the mean velocity) and for signals obtained at several heights in the boundary layer, all of which are consolidated in figure 13. The dimension is highest for the iso-surface for the local mean velocity, and drops off on both sides. Further, the peak value of the dimension goes up slowly towards 3 as the distance from the wall increases (see inset).

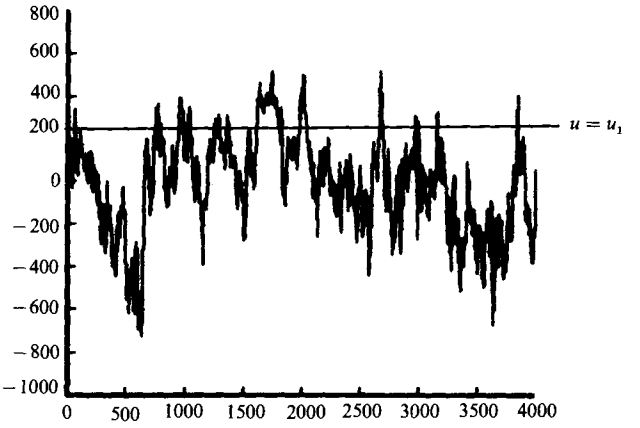

FIGURE 11. A turbulent velocity signal, $u(t)$, and the level u_1 defining the iso-velocity surface. The units are arbitrary.

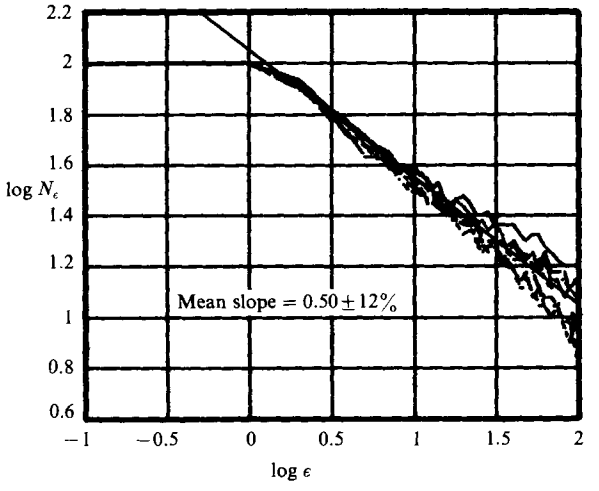

FIGURE 12. The logarithm (to base 10) of the number N_ϵ of the line segments of length ϵ required to cover the Cantor discontinuum obtained by the intersection of the threshold level u_1 ($= 0.75\ U_\infty$) with the velocity signal; $y/\delta = 0.35$, $U_\infty = 20$ m s^{-1}, $\delta = 4$ cm. Each line in the figure corresponds to a different segment of the velocity signal, each of which is of the order of 100 transverse integral scales long (see text). The mean slope (D_1) is 0.50 with a variation of $\pm 12\,\%$, giving a $D_3 = 2.50$.

A complete interpretation of these curves must take into account several factors. We expect the dimension to be largest for the most space-filling iso-velocity surface, or the velocity with the largest number of 'level crossings' (which roughly translates as the largest probability density – see, for example, Sreenivasan, Prabhu & Narasimha 1983). In the fully turbulent regions of the boundary layers, the peak of the probability density of the velocity signal occurs roughly at the mean velocity. Far into the boundary-layer free stream (i.e. $y \gg \delta$), we should ideally expect nothing but the free-stream velocity to prevail everywhere; thus the set $u_1 \neq U_\infty$ is a null set and its complement, namely the set $u_1 = U_\infty$, is really a classical volume for which the dimension must equal 3. In practice, the presence of some overriding noise on the free-stream velocity will reduce the peak dimension to something smaller than 3 and produce a spread onto the neighbouring velocity levels. In the intermittent regions, where laminar chunks of signal are interspersed between the turbulent ones, the

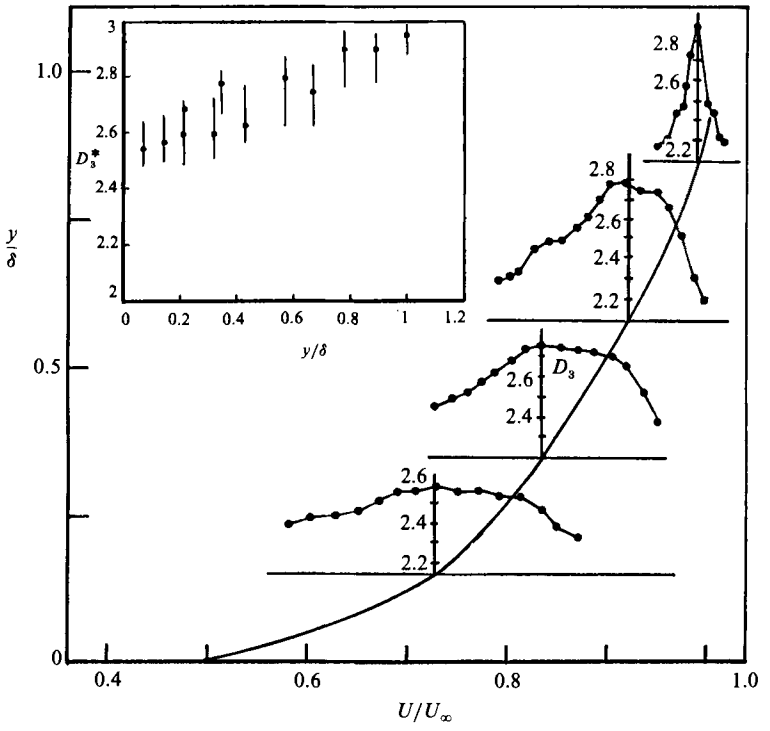

FIGURE 13. The dependence of the dimension of iso-surfaces of streamwise velocity as a function of both its magnitude and the distance from the wall. The spread is smaller as one goes away from the wall, while the peak magnitude D^* (shown in the inset) increases. The solid curve with no data is the mean velocity distribution in the boundary layer. The scales for the abscissae for each of the dimension plots is the same as that for the mean velocity.

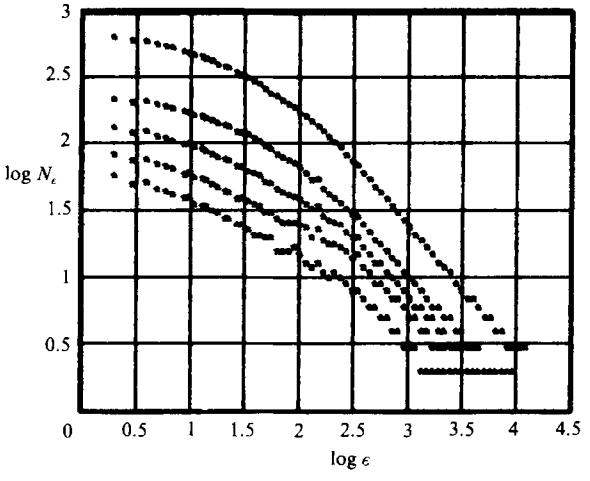

FIGURE 14. The effect of increasing the data segment length used for computing the dimension. The data segment length is, from bottom to top: 50ℓ, 83ℓ, 132ℓ, 200ℓ and 430ℓ, where ℓ is the transverse integral lengthscale. For small lengths, there is a distinct constant-slope region over the scales of interest; this becomes less conspicuous as the signal length increases. For large data segments, one can find a constant-slope region in the scale region far larger than the integral scale; the dimension D_1 is very nearly 1, however.

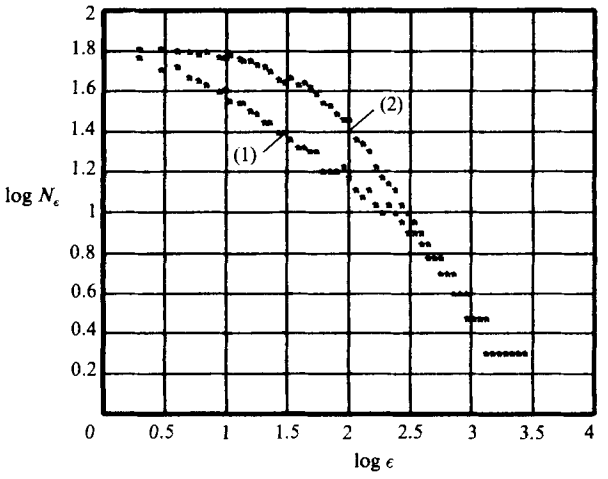

FIGURE 15. The box-counting algorithm applied to a typical iso-velocity intersection, curve (1), and to the same amount of points randomly distributed on a line, curve (2). For curve 2 there is no self-similarity range; only at large scales, for which the set looks like a solid line, do we get $D_1 = 1$.

dimension of an iso-velocity surface must be a weighted average between those of the same iso-surface in the turbulent and non-turbulent regions; the dimension will now peak at around the mean velocity in the non-turbulent region because the distribution of the Cantor-set elements is much denser there than anywhere else (with or without noise); according to the measurements of Kovasznay, Kibens & Blackwelder (1970), the mean velocity in the non-turbulent region is approximately the same as the overall mean velocity (at least to the accuracy appropriate in this context). It is also logical that the dimension must get smallest near the wall because the strong viscous effects will inhibit excessive contortions of an iso-velocity surface. While all these interpretations are consistent with the data of figure 13, note that the data of figure 13 do not apply to iso-surfaces in the non-turbulent regions only, and hence cannot answer questions related, for example, to the dimension of an iso-velocity surface with $u_1 = 0.9U_\infty$ residing entirely in the non-turbulent region.

In figures 12 and 13, we have used many segments of signal that are of the order of 50 transverse integral timescales long, and ensemble averaged over them. This should be quite acceptable because all iso-surfaces are only a few integral scales in streamwise extent and smaller in the transverse direction. We should point out, however, that if one uses fewer longer chunks of the signal for the calculations (the total length remaining the same), the straight-line regions become more and more ambiguous, until they disappear altogether for signal lengths beyond, say, 500 integral scales long (figure 14). The distribution then takes the shape characteristic of a random process (figure 15). What this implies is that the iso-surfaces are fractal-like when viewed on timescales of the order of 50 integral timescales, but behave more akin to random processes when viewed on timescales an order of magnitude larger.

An operationally helpful comment on the long-time randomization of the self-similar behaviour observed over short times is the following. If two separate segments of data show fractal characteristics but with slightly different fractal dimensions, it is easy to see that the sum of the two segments of data will in general *not* show the fractal behaviour. (The sum of two processes, each of which is hyperbolically

distributed, will also be hyperbolically distributed only if the scaling exponent is the same for both.) The observed randomization is a rough consequence of the central-limit theorem for the collection of a large number of slightly different and nearly independent events. If we argue that fractals are intermediate between complete order and total chaos, we may interpret our findings as revealing short-time order (or order over small extent) and long-time disorder in turbulence – a concept that has support in a variety of circumstances in turbulent flows.

4. Fractal dimensions of dissipative structures of turbulence

Another aspect of turbulence that is a candidate for fractal description is its dissipative (or internal or small) structure. It is known (Batchelor & Townsend 1949) that the small structure of turbulence is intermittent, and that scale-similarity arguments (e.g. Gurvich & Yaglom 1967) are very helpful in describing it. The essence of scale-similarity arguments in this context is the following. Within a given field of (fully developed) turbulence, consider a cube with sides of length L_0, where L_0 is an integral scale of turbulence. If we divide this cube into a number ($n \gg 1$) of smaller cubes of length $L_1 = L_0 n^{-\frac{1}{3}}$, the density of dissipation rate in each of these smaller cubes is distributed according to a certain probability law. Further subdivision of these cubes into second-order cubes of length $L_2 = L_1 n^{-\frac{1}{3}}$ leaves the probability distribution unaltered. This similarity extends to all scales of motion until one reaches sizes directly affected by viscosity. The simplest distribution is the binary one according to which a given high-order box either contains dissipation or does not. It is this simple picture that we shall pursue. The goal in this section is to examine the appropriateness of fractal description for the dissipative structure of both turbulent energy and of a passive-scalar field. Except for the material in the following subsection, which is an update of some earlier work, the rest of the material in this section is new.

4.1. *An update of Mandelbrot's work*

Let $\mathscr{D}$ be the fractal dimension of the dissipative field. (We shall avoid using the subscript 3 in this instance because there is no ambiguity.) When we have resolved the smallest scales η, and determined the number N of boxes of size η required to cover the entire dissipation regions, $\mathscr{D}$ can be calculated according to its definition:

$$\mathscr{D} = \frac{\log N}{\log (L_0/\eta)} \quad \text{or} \quad N = (L_0/\eta)^{\mathscr{D}}. \tag{4.1}$$

Since each cube has a volume of the order $(L_0/\eta)^3$, the total volume occupied by the cubes of active dissipation is $(L_0/\eta)^{\mathscr{D}-3}$. Since all dissipation is contained in these cubes, the level of dissipation in them is $(L_0/\eta)^{3-\mathscr{D}}$ times the global average value. Assuming local isotropy, this means that $(\mathrm{d}u/\mathrm{d}x)^2$ in the dissipating cubes is $(L_0/\eta)^{3-\mathscr{D}}$ times the global mean. Consequently, the kurtosis (or the flatness factor) of $\mathrm{d}u/\mathrm{d}x$, defined as

$$K = \overline{\left(\frac{\partial u}{\partial x}\right)^4} \Big/ \overline{\left(\frac{\partial u}{\partial x}\right)^2}^2 \tag{4.2}$$

will be given by $(L_0/\eta)^{2(3-\mathscr{D})}$ times the volume occupied by the dissipating cubes. (Note that this assumes the identity of the set supporting dissipation and that

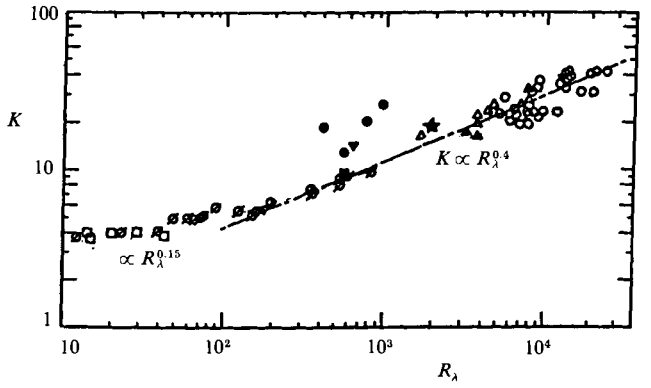

FIGURE 16. The variation of the kurtosis of (du/dt) as a function of the microscale Reynolds number. With minor modifications, this diagram is the same as figure 2 of Van Atta & Antonia (1980). □, Batchelor & Townsend (1947, 1949), grid turbulence; ■, Friehe, Van Atta & Gibson (1971), circular cylinder; ●, Gibson, Stegen & Williams (1970), atmosphere; ○, Wyngaard & Tennekes (1970), mixing layer and atmosphere; △, McConnell (1976), atmosphere; ▲, Park (1976), atmosphere; ◑, Williams & Paulson (1977), atmosphere; ▼, Champagne (1978), atmosphere; ⌀, Kuo & Corrsin (1971), grid turbulence and circular jet; ★, Pond & Stewart (1965), atmosphere.

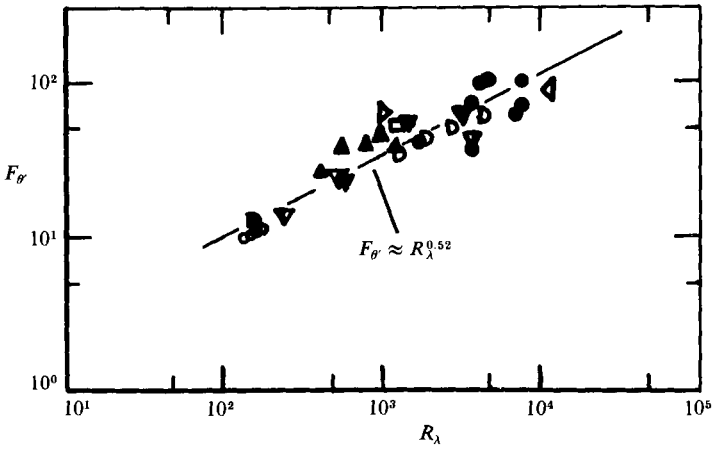

FIGURE 17. The kurtosis of the temperature derivative (dT/dt). ●, McConnell (1976), atmosphere; ◁, Antonia *et al.* (1980), atmosphere; ▷, Antonia & Danh (1977), atmosphere; ○, Sreenivasan, Antonia & Danh (1977), boundary layer; ▲, Gibson *et al.* (1970), atmosphere; ▷, Park (1976), atmosphere; □, McConnell (1976); jet; ▽, Antonia & Van Atta (1975); ◗, Antonia & Danh (1977), jet; ▽, Gibson & Masiello (1972), jet; ▼, Gibson *et al.* (1970), jet.

supporting $(du/dt)^2$. We are strictly calculating the fractal dimension of the latter.) From (2.4), we have

$$K \propto (L_0/\eta)^{3-\mathscr{D}} \propto R_\lambda^{\frac{3}{2}(3-\mathscr{D})}, \tag{4.3}$$

where $R_\lambda = u'\lambda/\nu$, λ being the Taylor microscale and u' the root-mean-square streamwise velocity. If we invoke Taylor's frozen-field hypothesis, the flatness factor of (du/dx) is the same as that of (du/dt); Antonia, Phan-Thien & Chambers (1980) have shown that this is true to within about 7%. A plot of $\log K$, where now K is the kurtosis of (du/dt), *vs.* $\log R_\lambda$ will yield the co-dimension $(3-\mathscr{D})$.

Mandelbrot used this argument and, from an examination of the kurtosis data from Kuo & Corrsin (1971), estimated $\mathscr{D}$ to be 2.6. More data have become available since

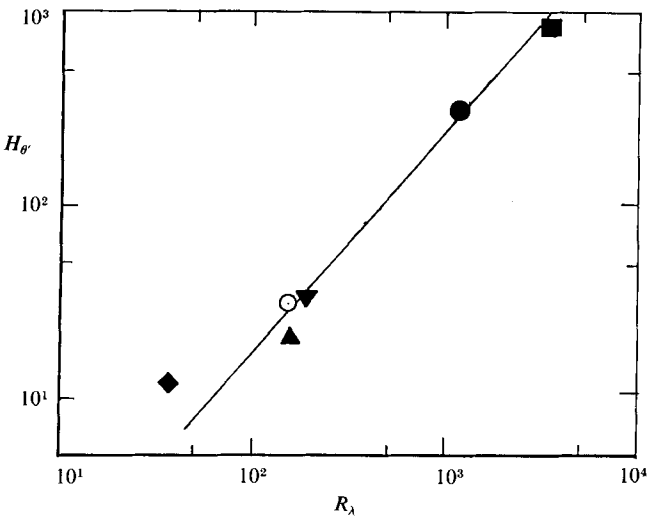

FIGURE 18. The hyperflatness of (dT/dt). ◆, Yeh (1971); ●, Sreenivasan, Antonia & Danh (unpublished), boundary layer; ▼, Antonia & Van Atta (1978), jet; ▲, Antonia & Van Atta (1978), laboratory boundary layer; ○, Antonia & Van Atta (1978), atmospheric boundary layer over land; ■, Park (1976), atmospheric boundary layer over water.

then, and are plotted in figure 16. With small modifications and additions, this figure is essentially a reproduction from Van Atta & Antonia (1980) who first compiled them. Given the difficulties in obtaining the data, they may be considered to collapse on a line with a slope of 0.4, yielding a $\mathscr{D}$ of 2.73, a revision from Mandelbrot's earlier estimate. This means that the fractional volume $(L_0/\eta)^{(\mathscr{D}-3)}$ occupied by the dissipation field is given by $(L_0/\eta)^{-0.27}$. For $R_\lambda < 150$, the slope in figure 16 is decidely smaller (≈ 0.15), which yields a $\mathscr{D}$ of 2.9. This indicates either that the dissipation regions at low Reynolds numbers are less spotty or that local isotropy does not obtain. Both are likely.

4.2. *Fractal dimension of the temperature 'dissipation' field*

Precisely the same arguments show that the kurtosis $F_{\theta'}$ for the temperature derivative (dT/dt) is related to the Reynolds number as

$$F_{\theta'} \propto R_\lambda^{\frac{3}{2}(3-\mathscr{D}^*)},$$

where $\mathscr{D}^*$ is the dimension of the temperature dissipation field. From figure 17, where all the available data have been collected, we conclude that $\mathscr{D}^* = 2.6$. (By drawing a line with a slope of 0.52 on figure 16, it is easy to see that the difference between the scalar and momentum dissipation fields is indeed statistically significant.) The temperature dissipation field (and by inference, those of all passive scalars) is less space filling ($\propto (L_0/\eta)^{-0.4}$), or is more intermittent. This result has been known to oceanographers for some time.

Similar arguments suggest that the so-called hyperflatness (i.e. the normalized sixth moment) of (dT/dt) must behave like $R_\lambda^{3(3-\mathscr{D}^*)}$. Figure 18 shows that this is quite consistent with the experimental data for $R_\lambda > 100$.

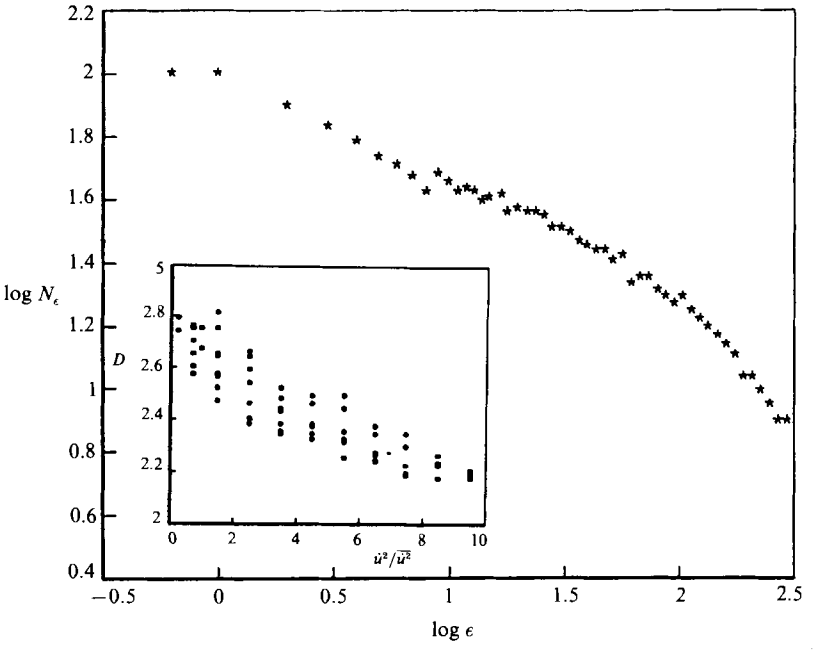

FIGURE 19. Log N_ϵ *vs.* log ϵ for the 'dissipation' field in grid turbulence by a line intercept using a threshold of $5\overline{u^2}$. The inset shows the dependence of the resulting dimension on the threshold used to identify the iso-dissipation surface.

4.3. *Dimensions of iso-dissipation surfaces by the line-intersection method*

It is obvious that the volume occupied by the dissipative structures depends on the threshold employed to identify the dissipation regions. There is no explicit mention of any threshold in the above method, which is both its strength and weakness – weakness because one does not really understand the inherent experimental definition of dissipation regions: the probes and the differentiation operations somehow set a threshold of their own. To permit sharper questions about the dependence on the threshold or, equivalently, about the dimensions of iso-dissipation surfaces, it is useful to resort to the line-intersection method. The method here is in principle free of some of the ambiguities raised in earlier sections because of the expected statistical isotropy of the dissipation regions, even in inhomogeneous shear flows. The procedure is exactly the same as in §2.4, except that we replace u by $(\mathrm{d}u/\mathrm{d}t)^2$. Figure 19 gives a typical result in grid turbulence for the threshold setting equal to 5 times the global mean value of dissipation. The slopes in the appropriate regions of similar curves obtained for various thresholds are shown in the inset. The fairly strong dependence of $\mathscr{D}$ on the threshold means that the dissipation regions identified by higher threshold settings are less space filling (obviously!), and the surfaces bounding them are less convoluted. (Similar data for clouds have now been obtained by Lovejoy & Schertzer 1986.) It must be mentioned that the range of scales over which self-similarity can be observed shrinks as we approach lower thresholds, thus making the dimension measurements more uncertain for iso-surfaces containing most of the dissipation (i.e. low threshold); this accounts for the larger scatter there. We observe however that the mean trend is to intercept the $\mathscr{D}$-axis at a value of near 2.7, which compares very well with the value obtained in §4.1.

We saw earlier that the volume occupied by the dissipation structures is small,

equal to $(L_0/\eta)^{\mathscr{D}-3}$. Fractal sets that occupy a small fraction of the embedding volume are called thin fractals (to be contrasted with fat fractals in §5.5). Mathematically, thin fractals are defined as sets possessing zero volume; in practice, this volume is positive but small because of the finite inner cutoff scale. We are justified in thinking of the dissipative set as a thin fractal because its volume/area ratio is vanishingly small at sufficiently high Reynolds numbers. Needless to say, the turbulent/non-turbulent interface is a thin fractal also.

5. Miscellaneous aspects

In this section, we shall briefly discuss several aspects of turbulence that may usefully be associated with fractals.

5.1. *Fractal dimension of interfaces in the developing region*

If we consider as an example the flow past a circular cylinder, the interface between the vortical and non-vortical regions in the immediate vicinity of the cylinder is expected to be a classical surface (because of the more or less regular vortex shedding), and the dimension will then be 2. This expectation will hold even at high Reynolds numbers except that it will be confined more and more near the 'origin' of the flow. Far downstream, we have shown the dimension of the interface to be about 2.4, which means that in the developing regions the dimension goes up from 2 to about 2.4. We have not made extensive measurements in this region, but scattered measurements (by imaging methods in jets and line cuts in wakes) confirm this suggestion. Naturally, the range of scale similarity is shorter.

5.2. *Evolution of material lines in grid turbulence*

To motivate the discussion here, it is convenient to refer to a 'classical' fractal, like a Koch curve (Mandelbrot 1982, p. 42). Iterations of the type shown in figure 20 on the sides of an initially equilateral triangle will produce smaller and smaller scales; the results of three iterations are shown. The fractal dimension of the boundary of the asymptotic object – the so-called Koch curve – can easily be deduced from its definition to be $\log 4/\log 3$. The relevant point here is that the length of this Koch curve increases exponentially with the number of iterations.

Suppose now that we place a patch of ink in a field of turbulence. The effect of turbulence dynamics, which is to distort the ink patch in a manner visualized schematically by Corrsin (1959), can be thought of as being equivalent to a repetitively occurring iteration scheme (according to some complex algorithm), producing smaller and smaller scales at each iteration. If this is so, the perimeter of the ink blob should increase exponentially. Mundane experimental difficulties have so far prevented us from demonstrating this expectation. However, we have examined a somewhat similar question of the growth of material lines in a turbulence field behind a grid. We generated lines of fine hydrogen bubbles in the developed region behind a grid placed in a water channel, and measured their length as they propagate downstream. Their true lengths have been measured by obtaining two orthogonal projections simultaneously (placing a mirror at 45°); the procedure is explained in the Appendix. Corrsin & Karweit (1969) had earlier measured the increase in length of hydrogen-bubble lines, but their method was indirect and used an equation (Corrsin & Phillips 1961) relating the length to the number of cuts experienced by sampling planes making all angles with the axis of a statistically axisymmetric line

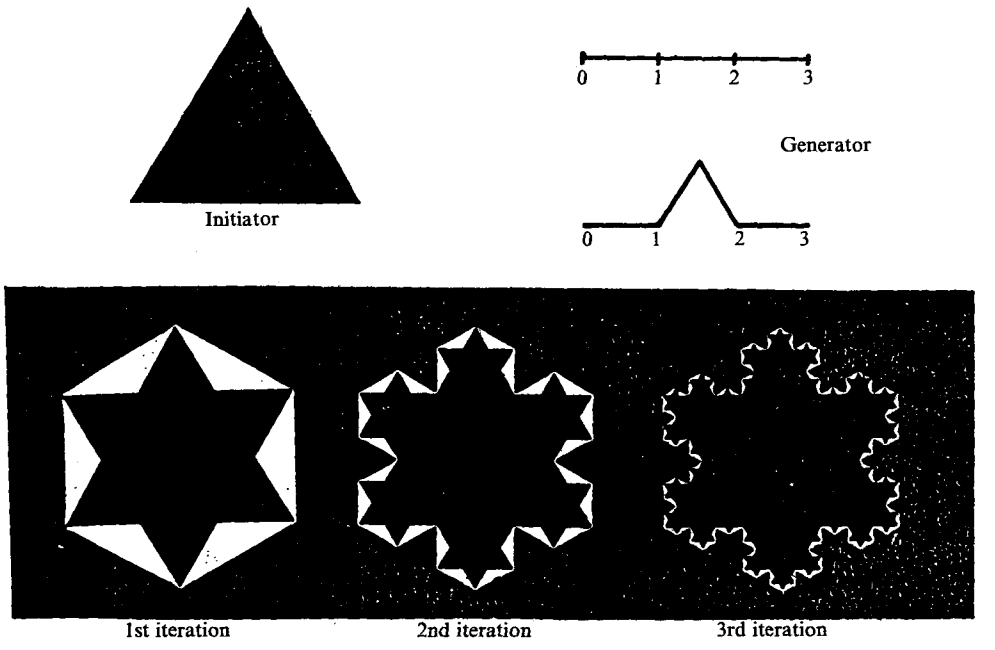

FIGURE 20. The iteration scheme for a triadic Koch island (Mandelbrot 1982) to be performed on an equilateral triangle (the so-called initiator); in each iteration the sides of the triangle are restructured according to the scheme shown on the upper right. The objects resulting from the first three iterations are shown.

element. It is gratifying to note that the two estimates agree where they overlap (figure 21). Clearly, except initially and in the last stages, the growth is indeed exponential. The initial behaviour is not expected to be exponential (Batchelor 1959), and the final levelling off is most likely due to the inadequate resolution of length measurement.

5.3. *Velocity signals*

Figure 22 shows the temperature signal taken on the centreline of a slightly heated axisymmetric jet (Sreenivasan *et al.* 1979). The most striking feature of this signal is the sharp ramp-like structures upon which the small structure is superimposed. Admittedly, this signal is carefully chosen to emphasize the point, but it is not statistically untypical. The temperature and velocity (especially normal component) signals in the boundary layer (even in the non-intermittent parts, see figure 11) show similar behaviour, although not as dramatic. The conclusion is that the fluctuations do not randomly jump about from one level to another, but gradually build up to a level from which they suddenly depart rather sharply. This behaviour is consistent with a power-law behaviour, which is symptomatic of self-similarity (and thus fractals). Following Lovejoy & Mandelbrot (1985), if we artificially construct a sum of randomly placed rectangular pulses whose width w obeys an inverse cumulative distribution $Pr(w > W) \propto W^{-1}$, and their height is $\pm w^{1/\alpha}$, the sign being randomly chosen, we can construct signals that show qualitative semblance to those shown in figure 22; here α is a characteristic exponent.

One useful comment relates to the expectation (Carter *et al.* 1986) that the turbulent signals themselves are fractals. This is obviously not a simple concept

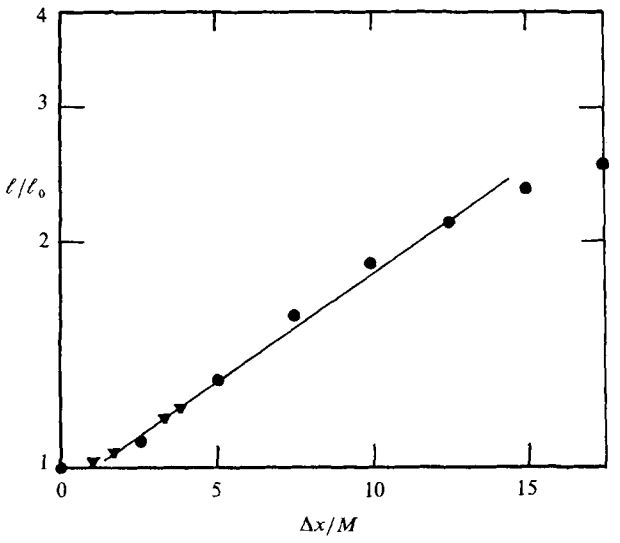

FIGURE 21. The average material line length as a function of the downstream distance from the grid. The circles are the data of Corrsin & Karweit (1969), the triangles the present. For both experiments, the hydrogen bubble lines were generated approximately 18 mesh sizes downstream of the grid.

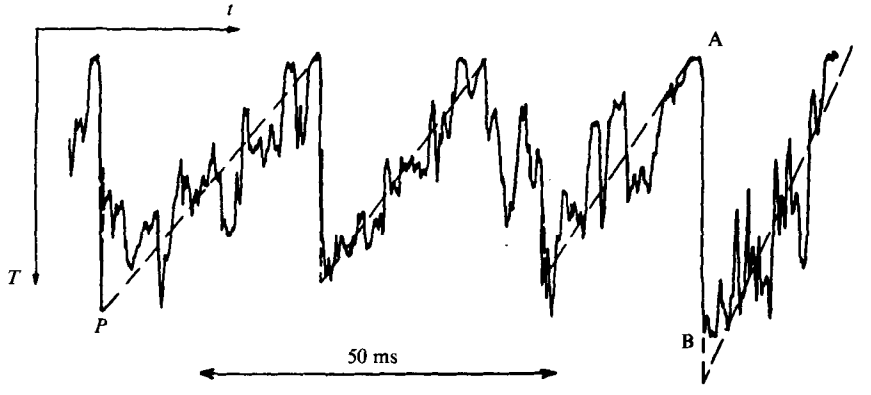

FIGURE 22. A temperature oscillogram in an axisymmetric heated jet, obtained in the region of maximum production of turbulent energy. Intermittency factor = 0.93. The sharp jumps associated with AB (for instance) have been a subject of much study.

because any dimension calculations depend strongly on the scales chosen for plotting the velocity signal. For example, if the signal is expanded to scales comparable with Kolmogorov scales, the signal looks very smooth leading to a dimension close to unity. The expectation is that the signals are self-affine fractals, by which we mean that there are more complex scaling behaviours (invariance under transformations of the type $S(x_1, x_2, \ldots, x_i) \rightarrow S(r_1 x_1, r_2 x_2, \ldots, r_i x_i)$, where all the r are different), and our work in this direction is continuing.

5.4. *Higher-order dimensions*

For the fractal description to be complete, one should be able at least to distinguish between two different fractals which may have the same dimension. Higher-order

dimensions are defined for this purpose (Hentschel & Procaccia 1983; Mandelbrot 1986), and are given by

$$D_q = \lim_{\epsilon \to 0} \left(\frac{1}{q-1} \frac{\log \Sigma\, p_i^q}{\log \epsilon} \right), \tag{5.1}$$

where p_i is the probability of finding points of the set in the ith box of length ϵ. For high values of q, D_q indicates the scaling behaviour of the more 'concentrated' regions; for low q, the character of the more 'sparse' regions is quantified. We have calculated these dimensions for several values of q, and these do display (as will be reported elsewhere) global characteristics similar to many strange sets discussed, for example, by Halsey *et al.* (1986).

5.5. *Fat fractals and turbulence*

At this stage, it is interesting to make some tentative connections between turbulence and what have been called fat fractals. In the literature, there is no apparent agreement on the precise meaning of fat fractals (contrast Umberger & Farmer 1985 with Grebogi *et al.* 1985), and this has to some extent dampened our own pursuit in this direction. At a basic level, however, the meaning of a fat-fractal set is that it occupies a finite volume (the box-counting algorithm applied to this set yields the dimension of the embedding space), but its boundary is a thin fractal. A possible example of a fat fractal is the set of all points in figure 3 where the smoke concentration is above a prescribed threshold; if the threshold properly sets apart the turbulent and non-turbulent regions, the 'skin' of the set is the interface whose dimension we have already measured in §2. Using a suitable integral of the measured intermittency factors in several standard turbulent flows, we have obtained rough estimates for the volume (say, within the region $U < 0.99\ U_\infty$) occupied by the turbulent zone. The fraction of volume is about 0.5 for circular jets (with or without coflow), about 0.6 for plane wakes behind circular cylinders, and about 0.75 for the two-dimensional boundary layers in constant pressure. The somewhat larger value in the last case is consistent with the decreased intermittency near the wall.

The same argument can be extended to the set of points in space where a velocity component (see §3) is greater than a prescribed threshold u_1. The 'skin' of such a fat fractal is the u_1 iso-velocity surface.

6. Concluding remarks

We have shown that there are several facets of turbulent flows possessing fractal-like behaviour. We have measured fractal dimensions for some of them. The fractal dimension is only one measure of the properties of a fractal set, albeit the most important one, and higher-order dimensions (mentioned in §5.4) will help in specifying the fractal more completely.

It is necessary to remark that the present work falls far short of proving that 'turbulence is fractal' without need for qualifications and reservations. As discussed in various sections, the qualifications arise partly because of the limitations of the techniques employed; these can (and should) undoubtedly be bettered in the next generation of experiments. But it seems to us on the basis of the present measurements that turbulence (except perhaps for the dissipation field) genuinely loses its fractal-like behaviour when viewed on very long timescales. Thus, turbulence is perhaps a collection of a number of fractals each of which is slightly different. We think that this view can be reconciled roughly with the view of turbulence now in vogue as an ensemble of semi-organized motions.

While there is not much question that this work is interesting, its usefulness in better coming to grips with the hard issues of the 'turbulence problem' is less certain. In this context, we might interpret the 'turbulence problem' to mean the following: given the various fractal dimensions of several of its facets, how may one reconstruct the turbulent flow that generated them? We know of no serious enquiry of this sort being done in the context of turbulence, although some beginnings seem to have been made in a broader setting (Barnsley *et al.* 1986). Unless this issue is addressed, it is not clear how fractals will advance our understanding of turbulence dynamics. In fact, contrary arguments have often been advanced. A case in point is the description of the dissipation field. Its traditional description via either vortex lines, tubes or blobs, it is said, is physically more appealing than its new description as a thin fractal of dimension 2.7. Actually, this point of view is not quite correct because a satisfactory description via vortex elements that is in complete consonance with measurements has never been attained (Kuo & Corrsin 1972). At any rate, fractals may describe the geometry of turbulence (keep in mind all our disclaimers at different places!), but geometry and dynamics do not have a one-to-one correspondence.

It is appropriate to contrast the measurement difficulties in obtaining fractal dimensions in physical space with those in phase space. Even engineering flows (at low Reynolds numbers) possess attractors with fractal dimensions (Sreenivasan 1986), but their determination becomes extremely difficult and uncertain as the Reynolds number increases. In contrast, the determination of fractal dimensions in physical space becomes more definitive at higher Reynolds numbers.

As a final remark, we note that numerical work of the sort initiated by Chorin (1982), dedicated to questions on the dynamic evolution of vortex elements, will go some way in establishing possible connections between fractals and turbulence.

Our thanks must extend to David Aronstein who, as a summer student, laid the groundwork for part of the work reported in §2.1; to William van Altena for allowing us the use of his digitizer; to Paul Dimotakis for his permission to reproduce figure 4 and for his penetrating comments on an earlier draft; to Benoit Mandelbrot for commenting on the manuscript, and for providing the necessary impetus in the early stages of this work more than three years ago by refusing to believe KRS's negative conclusions of that time; to a number of colleagues (especially W. Van der Water, Celso Grebogi, Rick Jensen, and B.-T. Chu) whose encouragement we received at various times; to Mark Lee and Paul Strykowski for carefully reading the manuscript and commenting on it; to Ted Lynn for cheerfully putting up with interruptions to his own boundary layer work; to Jim McMichael who encouraged its pursuit under an AFOSR grant. The last stages of this work were supported by the National Science Foundation.

Appendix: Growth of material lines in grid turbulence

A small water channel was used and lines of hydrogen bubbles were produced at $x/M = 18$ behind a turbulence-generating grid (solidity = 0.42, mesh size 3 mm). Downstream, a mirror was placed at an angle of 45° with the horizontal direction, so that a camera placed directly over the flow could simultaneously take pictures of two (perpendicular) projections of the same hydrogen-bubble line. By discretizing both lines and some simple trigonometric relations, it is then easy to determine the real length of the line in three dimensions.

Suppose we have two projections $\mathscr{P}_1$ and $\mathscr{P}_2$ (see figure 23) of a line in space, and

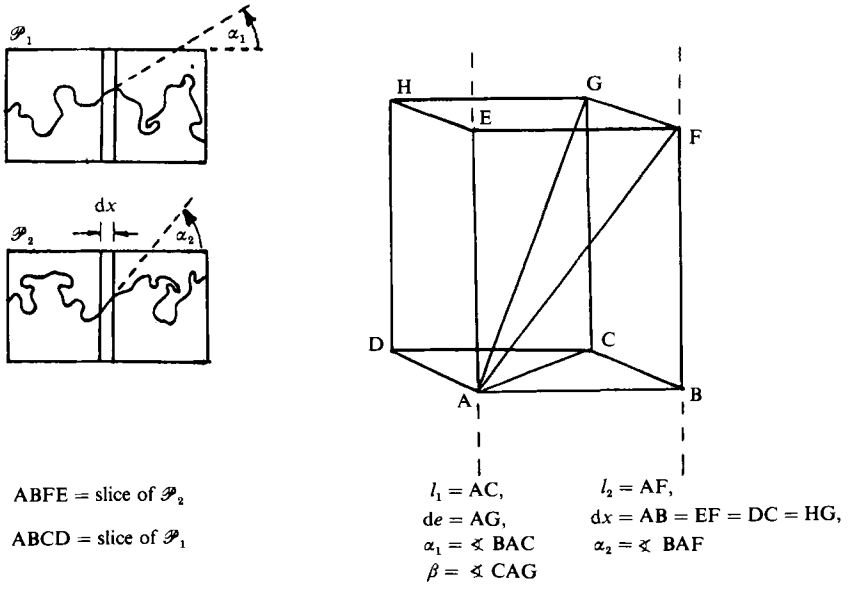

FIGURE 23. Orthogonal projections of a line segment and definition of angles and lines.

discretize them in equally spaced columns of width dx. From figure 23, the following relations can be inferred:

$$\mathrm{d}x = l_1 \cos\alpha_1 = l_2 \cos\alpha_2,$$

$$\mathrm{d}e \cos\beta = l_1,$$

$$\mathrm{d}e \sin\beta = l_2 \sin\alpha_2.$$

Thus,

$$\tan\beta = l_2 \sin\alpha_2 / l_1.$$

Finally, by expressing de as a function of dx and both angles, we get

$$\mathrm{d}e = \frac{\mathrm{d}x}{\cos\alpha_1 \cos(\arctan(\cos\alpha_1 \sin\alpha_2/\cos\alpha_2))}.$$

By measuring the angles α_1 and α_2 in each column of the discretized projections, and adding all the computed de, we get the real length (up to an accuracy of dx) of the line in three dimensions.

This was repeated for lines at several distances from the grid; resolution problems and fast diffusion of the hydrogen-bubble lines prevented us from analysing data at large distances.

REFERENCES

ANTONIA, R. A. & DANH, H. Q. 1977 *Phys. Fluids* **20**, 1050.

ANTONIA, R. A., PHAN-THIEN, N. & CHAMBERS, A. J. 1980 *J. Fluid Mech.* **100**, 193.

ANTONIA, R. A. & VAN ATTA, C. W. 1975 *J. Fluid Mech.* **67**, 273.

ANTONIA, R. A. & VAN ATTA, C. W. 1978 *J. Fluid Mech.* **84**, 561.

BARNSLEY, M. F., ERVIN, V., HARDIN, D. & LANCASTER, J. 1986 Solution of an inverse problem for fractals and other sets. *Proc. Natl Acad. Sci. USA* **83**, (to appear).

BATCHELOR, G. K. 1959 *J. Fluid Mech.* **5**, 113.

BATCHELOR, G. K. & TOWNSEND, A. A. 1947 *Proc. R. Soc. Lond.* A **190**, 534.

BATCHELOR, G. K. & TOWNSEND, A. A. 1949 *Proc. R. Soc. Lond.* A **199**, 239.

CARTER, P. H., CAWLEY, R., LICHT, A. L., YORKE, J. A. & MELNIK, M. S. 1986 In *Dimensions and Entropies* (ed. G. Mayer-Kress), p. 215. Springer.

CHAMPAGNE, F. H. 1978 *J. Fluid Mech.* **86**, 67.

CHORIN, A. 1982 *Commun. Math. Phys.* **83**, 517.

CORRSIN, S. 1959 *J. Geophy. Res.* **64**, 2134.

CORRSIN, S. & KARWEIT, M. 1969 *J. Fluid Mech.* **39**, 87.

CORRSIN, S. & KISTLER, A. L. 1954 *NACA Tech. Rep.* 3133.

CORRSIN, S. & PHILLIPS, O. M. 1961 *J. Soc. Indust. Appl. Maths* **9**, 395.

DIMOTAKIS, P., LYE, R. C. & PAPANTONIOU, D. Z. 1981 In *15th Intl Symp. Fluid Dyn., Jachranka, Poland.*

FEIGENBAUM, M. J. 1983 In *Nonlinear Dynamics and Turbulence* (ed. G. I. Barenblatt, G. Iooss & D. D. Joseph). Pitman Advanced Publishing Program.

FRIEHE, C. A., VAN ATTA, C. W. & GIBSON, C. H. 1971 In *Proc. of the AGARD Conf. on Turbulent Shear Flows, London, AGARD Conf. Proc.* **93**, 18–1.

GIBSON, C. H. & MASIELLO, P. 1972 In *Statistical Models and Turbulence* (ed. M. Rosenblatt & C. W. Van Atta), p. 427. Springer.

GIBSON, C. H., STEGEN, G. R. & WILLIAMS, R. B. 1970 *J. Fluid Mech.* **41**, 153.

GREBOGI, C., MCDONALD, S. W., OTT, E. & YORKE, J. A. 1985 *Phys. Lett.* **110A**, 1.

GURVICH, A. & YAGLOM, M. 1967 *Phys. Fluids Suppl.* **10**, S59.

HALSEY, T. C., JENSEN, M. H., KADANOFF, L. P., PROCACCIA, I. & SHRAIMAN, B. I. 1986 *Phys. Rev.* A**33**, 1141.

HENTSCHEL, H. G. E. & PROCACCIA, I. 1983 *Physica* **8D**, 435.

KIM, H. T., KLINE, S. J. & REYNOLDS, W. C. 1971 *J. Fluid Mech.* **50**, 133.

KOLMOGOROV, A. N. 1941 *C. R. Acad. Sci. URSS* **30**, 299.

KOLMOGOROV, A. N. 1962 *J. Fluid Mech.* **13**, 82.

KOVASZNAY, L. S. G., KIBENS, V. & BLACKWELDER, R. F. 1970 *J. Fluid Mech*, **41**, 283.

KUO, A.-Y. & CORRSIN, S. 1971 *J. Fluid Mech.* **50**, 285.

KUO, A.-Y. & CORRSIN, S. 1972 *J. Fluid Mech.* **56**, 477.

LOVEJOY, S. 1982 *Science* **216**, 185.

LOVEJOY, S. & MANDELBROT, B. B. 1985 *Tellus* **37A**, 209.

LOVEJOY, S. & SCHERTZER, S. 1986 Scale and dimension dependence in the detection and calibration of remotely sensed atmospheric phenomena. In *2nd Conf. on Satellite Meterology and Remote Sensing, Williamsburg, Va.* (submitted).

MANDELBROT, B. B. 1974 *J. Fluid Mech.* **62**, 331.

MANDELBROT, B. B. 1975 *J. Fluid Mech.* **72**, 401.

MANDELBROT, B. B. 1982 *The Fractal Geometry of Nature.* W. H. Freeman.

MANDELBROT, B. B. 1986 In *Dimensions and Entropies in Chaotic Systems* (ed. G. Mayer-Kress), p. 19. Springer.

MCCONNELL, S. O. 1976 The fine structure of velocity and temperature measured in the laboratory and the atmospheric marine boundary layer. Ph.D. thesis, University of California, San Diego.

MAXWORTHY, T. 1986 *J. Fluid Mech.* **173**, 95–114.

OBUKHOV, A. M. 1941 *C. R. Acad. Sci. URSS* **32**, 22.

OBUKHOV, A. M. 1962 *J. Fluid Mech.* **13**, 77.

ONSAGER, L. 1945 *Phys. Rev.* **68**, 286 (abstract only).

PARK, J. T. 1976 Inertial subrange turbulence measurements in the marine boundary layer. Ph.D. thesis, University of California, San Diego.

POND, S. & STEWART, R. W. 1965 *Izv. Atmos. Ocean. Phys.* **1**, 530.

RICHARDSON, L. F. 1922 *Weather Prediction by Numerical Process.* Cambridge University Press.

SREENIVASAN, K. R. 1986 In *Dimensions and Entropies in Chaotic Systems* (ed. G. Mayer-Kress), p. 222. Springer.

SREENIVASAN, K. R., ANTONIA, R. A. & BRITZ, D. 1979 *J. Fluid Mech.* **94**, 745.

SREENIVASAN, K. R., ANTONIA, R. A. & DANH, H. Q. 1977 *Phys. Fluids* **20**, 1238.

SREENIVASAN, K. R., PRABHU, A. & NARASIMHA, R. 1983 *J. Fluid Mech.* **137**, 251.

SUNYACH, M. & MATHIEU, J. 1969 *Intl J. Heat Mass Transfer* **12**, 1679.

TOWNSEND, A. A. 1956 *The Structure of Turbulent Shear Flows.* Cambridge University Press.

UMBERGER, D. & FARMER, J. D. 1985 *Phys. Rev. Lett.* **55**, 661.

VAN ATTA, C. W. & ANTONIA, R. A. 1980 *Phys. Fluids* **23**, 252.

WEIZSACKER, C. F. VON 1948 *Z. Phys.* **124**, 614.

WILLIAMS, R. M. & PAULSON, C. A. 1977 *J. Fluid Mech.* **83**, 547.

WYNGAARD, J. C. & TENNEKES, H. 1970 *Phys Fluids* **13**, 1962.

YEH, T. T. 1971 Spectral transfer and higher-order correlations of velocity and temperature fluctuations in heated grid turbulence. Ph.D. thesis, University of California, San Diego.